# Anatomy of topological Anderson transitions

Hao Zhang[1] and Alex Kamenev[1,2]
[1] *School of Physics and Astronomy, University of Minnesota, Minneapolis, Minnesota 55455, USA*
[2] *William I. Fine Theoretical Physics Institute, University of Minnesota, Minneapolis, Minnesota 55455, USA*

(Received 29 January 2023; accepted 30 November 2023; published 12 December 2023)

We study mesoscopic signatures of the topological Anderson transitions in topological disordered chains. To this end we introduce an integer-valued sample-specific definition of the topological index in finite-size systems. Its phase diagram exhibits a fascinating structure of intermittent topological phases, dubbed topological islands. Their existence is rooted in the real zeros of the underlying random polynomial. Their statistics exhibits finite-size scaling, pointing to the location of the bulk topological Anderson transition. While the average theories in AIII and BDI symmetry classes are rather similar, the corresponding patterns of topological islands and their statistics are qualitatively different. We also discuss observable signatures of sharp topological transitions in mesoscopic systems, such as persistent currents and entanglement spectra.

DOI: 10.1103/PhysRevB.108.224201

An interplay between topology and disorder plays an essential role in our understanding of topological materials [1–6]. Most notably it leads to a concept of topological Anderson insulators [7–45], where the robustness of the topological index is protected by the localized nature of wave functions, rather than a band gap in the energy spectrum. Phase diagrams of topological Anderson insulators generically exhibit transitions between localized phases with distinct topological indexes. Remarkably, localization length diverges at such transitions [11,20], indicating the presence of extended states. This happens even in one dimension, where the *ensemble averaged* theory in the thermodynamic limit is understood in terms of a two-parameter scaling [8,9], similar to a two-dimensional integer quantum Hall effect [46].

Although conceptually appealing, the average theory misses a trove of interesting information regarding sample-specific properties of disordered systems. The main goal of this paper is to uncover a fascinating hidden structure of intermittent topological phases, dubbed *topological islands*. Both the number of such islands and their locations on the phase diagram are determined by the real zeros of the underlying random polynomial and are completely lost in any ensemble-averaged treatment. A key step in this direction is a physically meaningful definition of an integer-valued topological index, which does not rely on the ensemble averaging nor on the thermodynamic limit (cf. Refs. [10,11,18,20]) .

We show that the finite-size scaling of the number of topological islands is a sensitive tool to reveal locations of the bulk topological Anderson transitions. Moreover, such finite-size scaling looks qualitatively distinct in different symmetry classes, e.g., AIII vs BDI, while their ensemble-averaged descriptions [9] are very much alike.

Our results are important for ongoing experimental efforts to detect one-dimensional topological phase transitions and localization-delocalization phenomena. In many real experiments, such as recent topological Anderson insulator observations [12], the system size is typically not large. As a result, self-averaged theories are less suitable for analysis. However, our results demonstrate what features one may expect in a real experiment setup, even when dealing with smaller systems. In the end, we discuss observable manifestations of topological transitions in mesoscopic-size-disordered samples [12,47] on persistent currents as well as entanglement spectra.

To illustrate the idea, let us consider a finite-size-disordered system defined on a ring,

$$H = \sum_{j=1}^{N} t_j c^{\dagger}_{j,A} c_{j,B} + t'_j c^{\dagger}_{j,B} c_{j+1,A} + \text{H.c.}, \tag{1}$$

where $c_{N+1,A} = c_{1,A}$. Here $A$ and $B$ label two sublattices and $t_j$ and $t'_j$ are hopping strengths within the unit cell and between nearest unit cells, respectively. The chiral-symmetry-preserving disorder is introduced as

$$t_j = m + W w_j, \quad t'_j = 1 + W' w'_j, \tag{2}$$

where $m$ is a uniform staggering, $W$ and $W'$ are the disorder strengths, and $w_j$ and $w'_j$ are independent random variables uniformly drawn from the box $[-1/2, 1/2]$. In all subsequent examples, $W' = \frac{1}{2}W$. The system possesses the chiral symmetry

$$\tau_z H \tau_z = -H, \tag{3}$$

where $\tau_z$ is the Pauli matrix acting in the sublattices' space. In the time-reversal-symmetric BDI class [6,48] all the parameters are real, while generalization to the AIII class is discussed below.

The usual topological index in the $k$ space cannot be defined in a finite-size and translationally noninvariant system. To overcome it we introduce a flux, threading the ring [8,49], through the substitution

$$t_N c^{\dagger}_{N,B} c_{1,A} \to t_N e^{i\phi} c^{\dagger}_{N,B} c_{1,A}. \tag{4}$$

The energy spectrum consists of $2N$ particle-hole symmetric "bands" as functions of flux $\phi \in [0, 2\pi]$. One can now

 

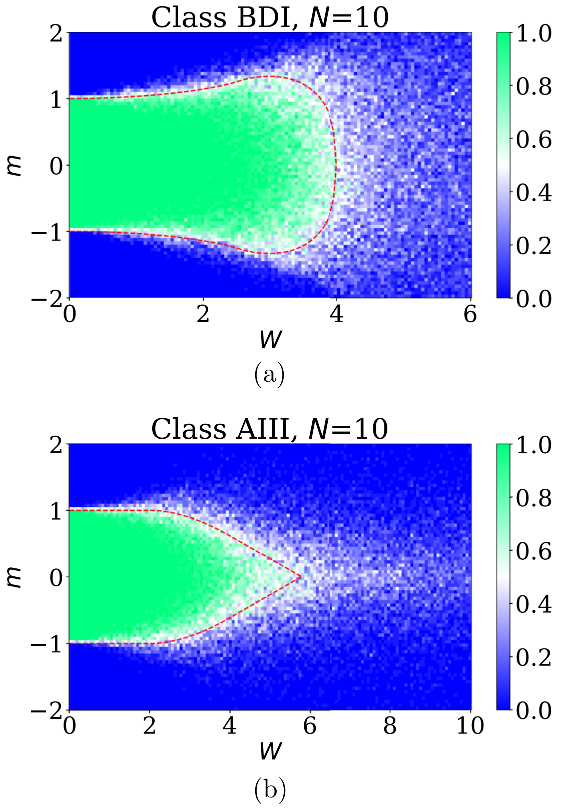


FIG. 1. Average topological index on the $(W, m)$ phase diagram for $N = 10$. To emphasize fluctuations, each point is averaged using a small sample size of 20. The red lines are the phase boundaries of the corresponding infinite systems. (a) Class BDI. (b) Class AIII.

introduce the index by using the Hamiltonian in a chiral basis,

$$H(m, \phi) = \begin{pmatrix} 0 & Q(m, \phi) \\ Q^\dagger(m, \phi) & 0 \end{pmatrix}, \tag{5}$$

and defining

$$\nu = \frac{1}{2\pi i} \int_0^{2\pi} d\phi \; \partial_\phi \log \det Q(m, \phi). \tag{6}$$

Since this is a winding number of the $\phi \mapsto \det Q(m, \phi)$ map, the index is integer valued.

A transition point, $m = m_c$, is marked by the gap at zero energy closing for some $\phi = \phi_{m_c}$. At this instance there are two zero energy eigenvalues, which implies $\det H = -|\det Q|^2 = 0$. This means that, as $\phi$ goes from 0 to $2\pi$, $\det Q(m_c, \phi)$ draws a closed loop in the complex plane which passes through the origin. Its winding number is thus undefined, while for $m \neq m_c$ it is an integer, which jumps by one over the transition. For the BDI class, $\phi_{m_c}$ is either 0 or $\pi$ due to the time-reversal symmetry.

Figure 1 shows the topological index for $N = 10$, averaged over 20 disorder realizations, on the phase plane of $(W, m)$. The red line is the topological phase boundary of the corresponding infinite system, which is calculated using the method of Ref. [11]. The enhanced fluctuations can be seen around the boundary. Notice that, in a certain region, they extend far beyond the bulk boundary to a very strong disorder.

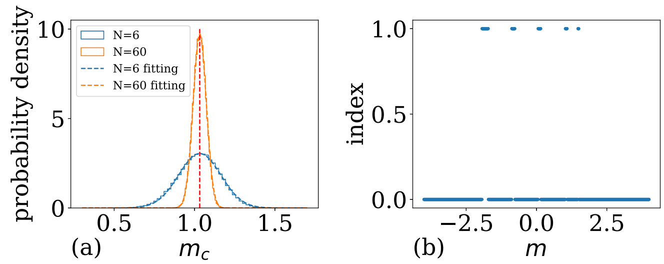


FIG. 2. (a) The distribution over $10^5$ realizations of the transition points near $m = 1$ for $W = 1$; $N = 6$ and $N = 60$ are shown in blue and orange along with the Gaussian fits. (b) Topological index for a system with $N = 6$, $W = 4$, and a fixed disorder realization. Notice five intermittent topological phases, dubbed topological islands.

In the weak disorder region, each realization exhibits two transition points located near $m \approx \pm 1$. The sample-to-sample fluctuations of each of these transition points [Fig. 2(a)] are well fitted by the Gaussian distribution. Its center follows the red boundary, while the width shrinks as $N \to \infty$. This marks a self-averaging transition.

However, when the disorder is strong, the fluctuations persist even in the $N \to \infty$ limit. This is attributed to the hidden structure of topological islands—the intermittent topological phases. Figure 2(b) shows a sample-specific topological index as a function of $m$ for $W = 4$. The number of topological islands can be as large as $N$. They do not disappear in the $N \to \infty$ limit but their width and relative area scales to 0.

For a better view of topological islands, the phase diagrams for fixed disorder realizations are shown in Fig. 3. The disorder realizations are fixed except the overall amplitude, $W$. The green region is topological, while the blue one is trivial. The red lines are the phase boundary of the corresponding infinite systems. The bulk topological region of the BDI model grows into $N$ topological islands. These islands extend to an arbitrarily strong disorder. Towards a weaker disorder they thicken and coalesce, ultimately forming the bulk topological region.

The presence of topological islands is a general feature, not restricted to the particular model we examined. They are determined by the real zeros of the random polynomial

$$p(m, \phi) = \det Q(m, \phi). \tag{7}$$

Here, $\phi$ takes all possible values. Those zeros are the boundaries of the islands and can be used to determine the number and locations of them. Topological islands exist as long as there are many real zeros of $p(m, \phi)$. Let us consider a general random BDI model with all ranges of longer hopping. We first introduce the control parameter $m$ as the hopping within the unit cell and thus $m$ is the diagonal element of $Q$. Then we introduce random hopping between different sites while respecting the chiral symmetry. $Q$ may be modeled as $mI + R$, where $I$ is the identity matrix and $R$ is a random matrix. Real zeros of $p(m, \phi)$ are thus the same as real eigenvalues of $R$ (up to a minus sign). There are around $\sqrt{N}$ real eigenvalues of $R$, where $N$ is the number of unit cells [50]. For class BDI, $\phi$ takes 0 and $\pi$, which leads to $2\sqrt{N}$ transitions. Hence, we

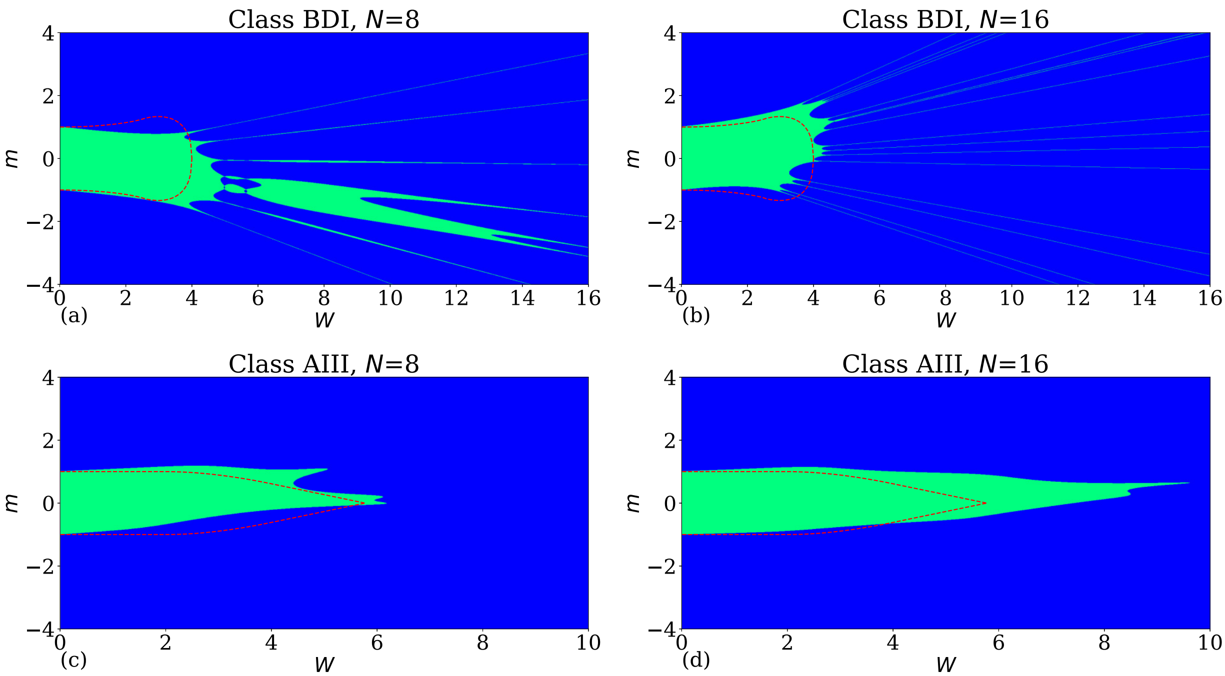


FIG. 3. Phase diagrams of fixed disorder realizations. The green region is $\nu = 1$, while the blue region is $\nu = 0$. The red lines are the phase boundaries of the corresponding infinite systems [11]. (a) and (b) Class BDI with $N = 8$ and $N = 16$. (c) and (d) Class AIII with $N = 8$ and $N = 16$.

expect there are roughly $\sqrt{N}$ topological islands for a generic BDI model.

For the specific model we consider, real zeros can be found by requiring the product of the absolute value of all intraunit cell hopping strength equals that of interunit cell hopping strength, $\prod_{j=1}^{N}|t_j| = \prod_{j=1}^{N}|t'_j|$. In the bulk of $\nu = 0$ (blue) region, $\prod_j |t_j| > \prod_j |t'_j|$. The radiating shape of topological islands can be understood by looking at the special points where the chain is accidentally cut in two, given that one of $t_j = 0$,

$$m + W w_j = 0. \tag{8}$$

Real zeros of the random polynomial are usually near them for large $W$. These straight lines on the $(W, m)$ plane, with a set of random slopes $-w_j$, mark the centers of the islands. The width of $\nu = 1$ (green) region around each such a line may be estimated for $W \gg 1$ as [51],

$$\Delta m_j = W w'_j \left(\frac{1}{2}\right)^{N-1} \prod_{i \neq j}^{N} \left(\frac{w'_i}{w_i - w_j}\right). \tag{9}$$

Thus, the angular width of the island, $\Delta m_j / W$, is a fixed number for a given realization. It decreases exponentially with $N \to \infty$.

To further understand the anatomy of the topological islands, we look at the number of islands [51] across all $m$'s for a fixed $W$ [Fig. 4(a)]. A convenient way to represent data is to plot $\frac{N_{\text{islands}}-1}{N-1}$ vs $W$. As $N$ increases it approaches a limiting function, smoothly interpolating between zero and one. To detect the exact location of the transition we look for the variance of the number of islands (divided by $N - 1$) [see the inset in Fig. 4(a)]. It shows that as $N$ increases, the variance peak become more narrow and centered at $W_c = 4$.

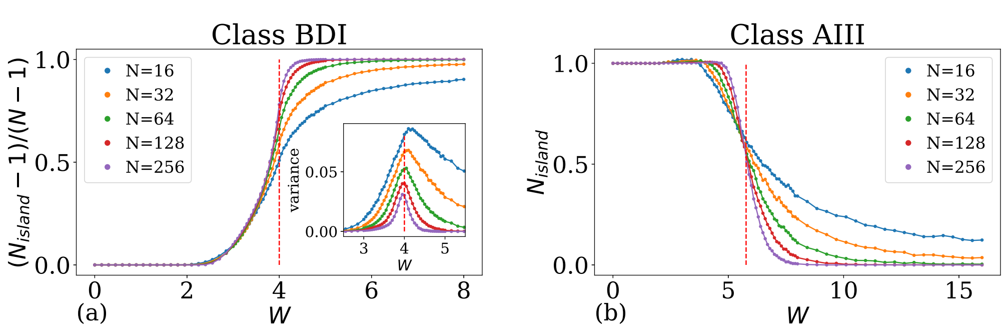


FIG. 4. The average number of islands versus the disorder strength $W$ for systems with different system sizes $N$. (a) Class BDI, the convenient quantity is $\frac{N_{\text{islands}}-1}{N-1}$. Inset shows its variance, which peaks at $W_c = 4$ as $N \to \infty$. (b) Class AIII, the graphs shows a crossing point at $W_c = 4/\log(2)$.

This illustrates that the bulk transition point for $m = 0$ may be identified as the maximum of the variance of the number of islands in a finite-size simulation.

We turn now to the AIII symmetry class with the broken time-reversal symmetry. To this end we use Hamiltonian Eq. (1) with the complex hopping amplitudes. Namely, the absolute values and phases of $w_j$ and $w'_j$ are now uniformly drawn from $(0, 1/2)$ and $(-\pi, \pi)$, respectively. Figure 1(b) shows the average phase diagram of class AIII. It is similar to that of BDI class and so is the average theory of the corresponding bulk topological Anderson transition [8,9,11,20]. The latter takes place along the red line, where the localization length diverges.

However, the sample-specific fluctuations of the topological index behaves in a way that is very different from the BDI class. Indeed, the topological islands now have a finite extent and are limited to a relatively weak disorder part of the phase diagram [Figs. 3(c) and 3(d)]. Moreover, there are only a few islands and their number does not increase with $N$. This is due to complex random hopping amplitudes which statistically exclude instances of a cut chain (real and imaginary parts do not vanish at the same $W$). The average number of islands across all $m$'s is plotted in Fig. 4(b) for different system sizes $N$. It shows a well-defined crossing point at $W_c = 4/\log(2)$, in agreement with the bulk transition point at $m = 0$ [11]. As $N$ grows, the number of islands approaches 1 and 0 for $W < W_c$ and $W > W_c$, correspondingly.

We have shown that mesoscopic sample-to-sample fluctuations manifest themselves in the formation of topological islands. Their number, shape, and statistics are qualitatively different between BDI and AIII classes. However, in both cases their finite-size scaling provides the exact location of the corresponding bulk topological Anderson transition.

Before concluding we discuss observable signatures of the *sharp* topological transitions in finite-size systems.

First, consider a mesoscopic persistent current, given by [52–55]

$$I(m, \phi) = -\partial_\phi E(m, \phi), \tag{10}$$

where $E(m, \phi)$ is the ground-state energy of the half-filled system. It is a periodic function $\phi$, which exhibits a maximum at a certain $\phi$, $I_{\max}(m) = \max_\phi I(m, \phi)$. It appears that this maximal value exhibits a nonanalytic maximum at the topological transition critical $m_c$ [Fig. 5(a)],

$$I_{\max} \propto -|m - m_c|^\alpha, \tag{11}$$

where $\alpha$ is the critical exponent that may have dependence on system parameters.

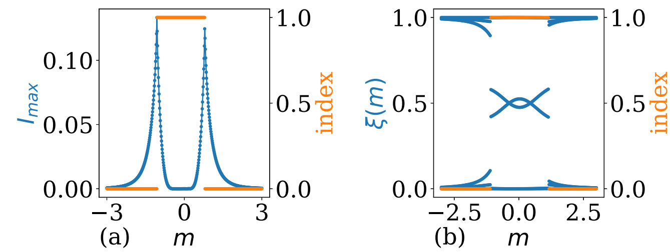


FIG. 5. (a) Sample-specific maximum value of the persistent current $I_{\max}$ (blue dots) and the topological index $\nu$ (orange dots) as functions of $m$. $I_{\max}$ peaks at the two transition points with power-law singularities. (b) The entanglement spectrum of a BDI realization with $N = 6$ and $W = 1$. The blue dots are $\xi_i$, which are related to the entanglement energies through Eq. (13). The orange dots are the topological index. The entanglement spectrum has discontinuities at transitions. In the topological phase, there are two $\xi_i$ around 0.5 (and thus $\epsilon_i$ around 0).

In simple models with nearest-neighbor hopping, there are zero energy states located close to weak links in topological phases and they resemble the edge states while in more general models, their localization cannot be tight to any visible edge.

The transitions also have implications in entanglement spectra [10,56]. We divide the chain into two equal parts $A$ and $B$ (do not confuse with the sublattices) and calculate the trace over the $B$ part. The corresponding reduced density matrix of $A$ takes the form

$$\rho_A = \sum_{n_B} \langle n_B|\rho|n_B\rangle \propto e^{-\sum_i \epsilon_i a_i^\dagger a_i}, \tag{12}$$

where $|n_B\rangle$ are basis vectors of the $B$ part and $a_i$ are normal modes. The second equality is a property of Gaussian (i.e., noninteracting) models [57]. Here $\epsilon_i$ is the entanglement spectrum, which may be expressed through the eigenvalues $\xi_i$ of the one-particle covariance matrix $C_{jj'} = \langle c_j^\dagger c_{j'}\rangle$ [57] as

$$\epsilon_i = \frac{1}{2} \log\left(\frac{1 - \xi_i}{\xi_i}\right), \tag{13}$$

where $j$ and $j'$ label the lattice sites of the $A$ part and $\langle \ldots \rangle$ denote ground-state averaging. The entanglement spectrum exhibits discontinuities at topological transitions [see Fig. 5(b)]. For a weak disorder, the spectrum also exhibits nearly zero entanglement energies within the topological phase. It can thus be considered as a means to identify the sharp topological transitions in mesoscopic systems.

We are grateful to Xuzhe Ying for useful discussions. This work was supported by the NSF under Grant No. DMR-2037654.

[1] B. A. Bernevig, *Topological Insulators and Topological Superconductors* (Princeton University, Princeton, NJ, 2013).
[2] J. K. Asbóth, L. Oroszlány, and A. Pályi, *A Short Course on Topological Insulators*, Lecture Notes in Physics, Vol. 919 (Springer, Cham, 2016).
[3] S.-Q. Shen, *Topological Insulators: Dirac Equation in Condensed Matters* (Springer, Berlin, 2017).
[4] X.-L. Qi and S.-C. Zhang, Topological insulators and superconductors, Rev. Mod. Phys. **83**, 1057 (2011).
[5] M. Z. Hasan and C. L. Kane, Colloquium: Topological insulators, Rev. Mod. Phys. **82**, 3045 (2010).

[6] C.-K. Chiu, J. C. Y. Teo, A. P. Schnyder, and S. Ryu, Classification of topological quantum matter with symmetries, Rev. Mod. Phys. **88**, 035005 (2016).

[7] J. Li, R.-L. Chu, J. K. Jain, and S.-Q. Shen, Topological Anderson insulator, Phys. Rev. Lett. **102**, 136806 (2009).

[8] A. Altland, D. Bagrets, L. Fritz, A. Kamenev, and H. Schmiedt, Quantum criticality of quasi-one-dimensional topological Anderson insulators, Phys. Rev. Lett. **112**, 206602 (2014).

[9] A. Altland, D. Bagrets, and A. Kamenev, Topology vs. Anderson localization: Nonperturbative solutions in one dimension, Phys. Rev. B **91**, 085429 (2015).

[10] E. Prodan, T. L. Hughes, and B. A. Bernevig, Entanglement spectrum of a disordered topological chern insulator, Phys. Rev. Lett. **105**, 115501 (2010).

[11] I. Mondragon-Shem, T. L. Hughes, J. Song, and E. Prodan, Topological criticality in the chiral-symmetric AIII class at strong disorder, Phys. Rev. Lett. **113**, 046802 (2014).

[12] E. J. Meier, F. A. An, A. Dauphin, M. Maffei, P. Massignan, T. L. Hughes, and B. Gadway, Observation of the topological Anderson insulator in disordered atomic wires, Science **362**, 929 (2018).

[13] S. Stützer, Y. Plotnik, Y. Lumer, P. Titum, N. H. Lindner, M. Segev, M. C. Rechtsman, and A. Szameit, Photonic topological Anderson insulators, Nature (London) **560**, 461 (2018).

[14] C. W. Groth, M. Wimmer, A. R. Akhmerov, J. Tworzydło, and C. W. J. Beenakker, Theory of the topological Anderson insulator, Phys. Rev. Lett. **103**, 196805 (2009).

[15] D. D. Vu and S. Das Sarma, Weak quantization of noninteracting topological Anderson insulator, Phys. Rev. B **106**, 134201 (2022).

[16] T. A. Loring and M. B. Hastings, Disordered topological insulators via C*-algebras, Europhys. Lett. **92**, 67004 (2010).

[17] H. Jiang, L. Wang, Q.-f. Sun, and X. C. Xie, Numerical study of the topological Anderson insulator in HgTe/CdTe quantum wells, Phys. Rev. B **80**, 165316 (2009).

[18] E. Prodan, Disordered topological insulators: A Non-commutative geometry perspective, J. Phys. A: Math. Theor. **44**, 113001 (2011).

[19] Y. Xing, L. Zhang, and J. Wang, Topological Anderson insulator phenomena, Phys. Rev. B **84**, 035110 (2011).

[20] J. Song and E. Prodan, AIII and BDI Topological systems at strong disorder, Phys. Rev. B **89**, 224203 (2014).

[21] I. C. Fulga, F. Hassler, A. R. Akhmerov, and C. W. J. Beenakker, Scattering formula for the topological quantum number of a disordered multimode wire, Phys. Rev. B **83**, 155429 (2011).

[22] A. Haim and A. Stern, Benefits of weak disorder in one-dimensional topological superconductors, Phys. Rev. Lett. **122**, 126801 (2019).

[23] C.-B. Hua, R. Chen, D.-H. Xu, and B. Zhou, Disorder-induced Majorana zero modes in a dimerized Kitaev superconductor chain, Phys. Rev. B **100**, 205302 (2019).

[24] A. R. Akhmerov, J. P. Dahlhaus, F. Hassler, M. Wimmer, and C. W. J. Beenakker, Quantized conductance at the Majorana phase transition in a disordered superconducting wire, Phys. Rev. Lett. **106**, 057001 (2011).

[25] J. H. Bardarson, P. W. Brouwer, and J. E. Moore, Aharonov-Bohm oscillations in disordered topological insulator nanowires, Phys. Rev. Lett. **105**, 156803 (2010).

[26] C.-A. Li, B. Fu, Z.-A. Hu, J. Li, and S.-Q. Shen, Topological phase transitions in disordered electric quadrupole insulators, Phys. Rev. Lett. **125**, 166801 (2020).

[27] J. Claes and T. L. Hughes, Disorder driven phase transitions in weak AIII topological insulators, Phys. Rev. B **101**, 224201 (2020).

[28] M. M. Wauters, A. Russomanno, R. Citro, G. E. Santoro, and L. Privitera, Localization, topology, and quantized transport in disordered floquet systems, Phys. Rev. Lett. **123**, 266601 (2019).

[29] H.-C. Hsu, P.-M. Chiu, and P.-Y. Chang, Disorder-induced topology in quench dynamics, Phys. Rev. Res. **3**, 033242 (2021).

[30] S. Velury, B. Bradlyn, and T. L. Hughes, Topological crystalline phases in a disordered inversion-symmetric chain, Phys. Rev. B **103**, 024205 (2021).

[31] H. Liu, J.-K. Zhou, B.-L. Wu, Z.-Q. Zhang, and H. Jiang, Real-space topological invariant and higher-order topological Anderson insulator in two-dimensional non-Hermitian systems, Phys. Rev. B **103**, 224203 (2021).

[32] D. S. Antonenko, E. Khalaf, P. M. Ostrovsky, and M. A. Skvortsov, Mesoscopic conductance fluctuations and noise in disordered Majorana wires, Phys. Rev. B **102**, 195152 (2020).

[33] P. Titum, E. Berg, M. S. Rudner, G. Refael, and N. H. Lindner, The anomalous Floquet-Anderson insulator as a nonadiabatic quantized charge pump, Phys. Rev. X **6**, 021013 (2016).

[34] P. Titum, N. H. Lindner, M. C. Rechtsman, and G. Refael, Disorder-induced Floquet topological insulators, Phys. Rev. Lett. **114**, 056801 (2015).

[35] H.-M. Guo, G. Rosenberg, G. Refael, and M. Franz, Topological Anderson insulator in three dimensions, Phys. Rev. Lett. **105**, 216601 (2010).

[36] K. Kobayashi, T. Ohtsuki, and K.-I. Imura, Disordered weak and strong topological insulators, Phys. Rev. Lett. **110**, 236803 (2013).

[37] H. Jiang, Z. Qiao, H. Liu, J. Shi, and Q. Niu, Stabilizing topological phases in graphene via random adsorption, Phys. Rev. Lett. **109**, 116803 (2012).

[38] J. H. Garcia, L. Covaci, and T. G. Rappoport, Real-space calculation of the conductivity tensor for disordered topological matter, Phys. Rev. Lett. **114**, 116602 (2015).

[39] A. Yamakage, K. Nomura, K.-I. Imura, and Y. Kuramoto, Disorder-induced multiple transition involving $Z_2$ topological insulator, J. Phys. Soc. Jpn. **80**, 053703 (2011).

[40] J. Song, H. Liu, H. Jiang, Q.-f. Sun, and X. C. Xie, The dependence of topological Anderson insulator on the type of disorder, Phys. Rev. B **85**, 195125 (2012).

[41] S. Ryu and K. Nomura, Disorder-induced metal-insulator transitions in three-dimensional topological insulators and superconductors, Phys. Rev. B **85**, 155138 (2012).

[42] D.-W. Zhang, L.-Z. Tang, L.-J. Lang, H. Yan, and S.-L. Zhu, Non-Hermitian topological anderson insulators, Sci. China Phys. Mech. Astron. **63**, 267062 (2020).

[43] Y.-Y. Zhang, R.-L. Chu, F.-C. Zhang, and S.-Q. Shen, Localization and mobility Gap in topological Anderson insulator, Phys. Rev. B **85**, 035107 (2012).

[44] Y.-B. Yang, K. Li, L.-M. Duan, and Y. Xu, Higher-order topological Anderson insulators, Phys. Rev. B **103**, 085408 (2021).

[45] X. Shi, I. Kiorpelidis, R. Chaunsali, V. Achilleos, G. Theocharis, and J. Yang, Disorder-induced topological phase

transition in a 1D mechanical system, Phys. Rev. Res. **3**, 033012 (2021).

[46] A. Pruisken, On localization in the theory of the quantized Hall effect: A two-dimensional realization of the $\theta$-vacuum, Nucl. Phys. B **235**, 277 (1984).

[47] S. Barkhofen, S. De, J. Sperling, C. Silberhorn, A. Altland, D. Bagrets, K. W. Kim, and T. Micklitz, Experimental observation of topological quantum criticality, arXiv:2301.05428.

[48] A. Altland and M. R. Zirnbauer, Nonstandard symmetry classes in mesoscopic normal-superconducting hybrid structures, Phys. Rev. B **55**, 1142 (1997).

[49] I. C. Fulga, F. Hassler, A. R. Akhmerov, and C. W. J. Beenakker, Topological quantum number and critical exponent from conductance fluctuations at the quantum Hall plateau transition, Phys. Rev. B **84**, 245447 (2011).

[50] A. Edelman, E. Kostlan, and M. Shub, How many eigenvalues of a random matrix are real? J. Am. Math. So. **7**, 247 (1994).

[51] See Supplemental Material at http://link.aps.org/supplemental/10.1103/PhysRevB.108.224201 for the derivation and for the details of the numerical calculations.

[52] A. C. Bleszynski-Jayich, W. E. Shanks, B. Peaudecerf, E. Ginossar, F. v. Oppen, L. Glazman, and J. G. E. Harris, Persistent currents in normal metal rings, Science **326**, 272 (2009).

[53] S. Ghosh and A. Saha, Persistent current of relativistic electrons on a Dirac ring in presence of impurities, Eur. Phys. J. B **87**, 167 (2014).

[54] A. Nava, R. Giuliano, G. Campagnano, and D. Giuliano, Persistent current and zero-energy Majorana modes in a $p$-wave disordered superconducting ring, Phys. Rev. B **95**, 155449 (2017).

[55] D. Sticlet, B. Dóra, and J. Cayssol, Persistent currents in Dirac fermion rings, Phys. Rev. B **88**, 205401 (2013).

[56] H. Li and F. D. M. Haldane, Entanglement spectrum as a generalization of entanglement entropy: Identification of topological order in non-Abelian fractional quantum Hall effect states, Phys. Rev. Lett. **101**, 010504 (2008).

[57] I. Peschel, Calculation of reduced density matrices from correlation functions, J. Phys. A: Math. Gen. **36**, L205 (2003).